Solving curing-protocol-dependent shape errors in PDMS replication

Emilie Delplanque, Antoine Aymard, Davy Dalmas, Julien Scheibert

Solving curing-protocol-dependent shape errors in PDMS replication

Emilie Delplanque[1], Antoine Aymard[1], Davy Dalmas[1] and Julien Scheibert[1]

1 Univ Lyon, Ecole Centrale de Lyon, ENISE, ENTPE, CNRS, Laboratoire de Tribologie et Dynamique des Systèmes LTDS, UMR 5513, F-69134, Ecully, France

E-mail: julien.scheibert@ec-lyon.fr

Date: 25/07/2021

Abstract. PolyDiMethylSiloxane (PDMS) is an elastomer increasingly used to produce soft objects by replication, in a variety of fields including soft electronics, microfluidics, tribology, biomechanics and soft robotics. While the replication of nano- to micrometric scales is usually considered faithful, little is known about the replication quality on larger macroscopic scales. Here, we show that the top surface of parallelepipedic PDMS blocks, molded on a rigid plate, deviates from its expected planeity, the amplitude of the deviation being dependent on the crosslinking protocol. As a practical solution, we identify a suitable two-steps protocol which eliminates those replication errors. Using finite element simulations, we show that the effect originates from a thermal contraction when the sample cools from the curing temperature down to the operating temperature. This phenomenon actually applies at any length scale, and finely depends on the sample's aspect ratio and boundary conditions. Our results should help mitigating replication errors in all applications where a well-defined sample geometry is required.

Keywords: silicone rubber, Sylgard 184, shrinkage,

1. Introduction

PolyDiMethylSiloxane (PDMS) is a low cost elastomeric material combining large compliance, large toughness, good chemical resistance and biocompatibility. Sample preparation is relatively simple and usually involves crosslinking of the PDMS chains contained in a liquid mixture, inside a mold. In this respect, PDMS is usually deemed to enable good replication of the mold global shape and of the topographical features of its surfaces (roughness), down to the microscale, and even nanoscale. [1, 2, 3]. And indeed, it has been used for replication purposes in a variety of fields including lab-on-chip [4], soft electronics [5], microfluidics [6, 7], biomechanics [8], soft robotics [9], metamaterials [10] and tribology [11, 12, 13, 14].

The replication quality has mainly been investigated at small scales, micrometric and below [1]. In particular, it has been found that for the tiniest nanoscale features, the replication is more accurate when the crosslinked PDMS is stiffer and when,in its fluid state, it better wets the solid mold [15, 2, 3]. In contrast, the replication quality at large scales, millimeter or centimeter, remains largely unexplored. The issue is however crucial in some cases where a wide range of scales is of interest on the very same PDMS sample. As an example, Romero et al. [16] considered a centimetric, nominally flat sample, decorated by an array of microspheres with individual heights intended to be controlled at the micrometer scale. Unexpectedly, when that sample was pressed against a flat glass plate, the pressure field was found heterogeneous at the overall sample scale. This observation suggested that, while the invididual microspheres were accurately replicated, the macroscopic shape of the sample departed from the expected flatness, by an amount sufficient to modify significantly the desired microspheres height distribution.

In this context, we address here the question of PDMS replication quality at large scales, by preparing parallelepipedic samples directly on rigid plates, and investigating the deviations to flatness of their largest free surface. For the material, we focused on the most widely used PDMS in the scientific literature: Dow Corning's Sylgard 184. In the vast majority of cases, it is crosslinked in a single step at a fixed temperature, before demolding. The temperature value (from room temperature to 150 °C) and crosslinking duration (from a few minutes to several days) vary widely in the literature, as illustrated in Tab. 1.

Table 1: Various single-step curing protocols for PDMS Sylgard 184 in the literature.

Temperature (°C)	Time (min)	References
150	10	[17] [18]
150	30	[19]
100	60	[20]
100	180	[21]
85	120	[22]
85	180	[20]
80	120	[23]
80	300	[24]
75	1440	[25]
70	30	[26]
65	120	[27]
65	240	[20]
65	Overnight	[28] [29]
60	720(12hours)	[30]
Room Temperature	Overnight	[31] [32]
Room Temperature	9000(6.25 days)	[12]

Here, by testing various curing protocols, we will show that no single-step protocol is capable of ensuring both a satisfactory replication quality and a fully completed cross-linking reaction (Sec. 2). We then propose a two-steps curing protocol which solves those two problems at once (Sec. 3), and discuss the respective roles of the main aspects of this protocol (Sec. 4). Finally, we will identify thermal contraction as the physical origin of the replication errors observed with single-step protocols, and discuss its dependence on sample size, aspect ratio and boundary conditions (Sec. 5).

2. Identification of replication errors using single-step curing protocols

2.1. Sample preparation

A mold was first prepared out of an aluminum 2017 A block (30 mm×30 mm×12 mm). One face of the block was first prepared as a planar reference surface. Then, a 7.2 mm deep parallelepipedic cavity was excavated below that reference surface (see Fig. 1 for the dimensions), using a micro-milling machine (Minimill GX, Minitech) with a flat-ended tool of diameter 2 mm. The mold is then closed by pressing a lid made of a stack of three microscope glass slides (each of thickness 1 mm) on what remains of the reference plane, and held in place by two clips (red in Fig. 2). The stack

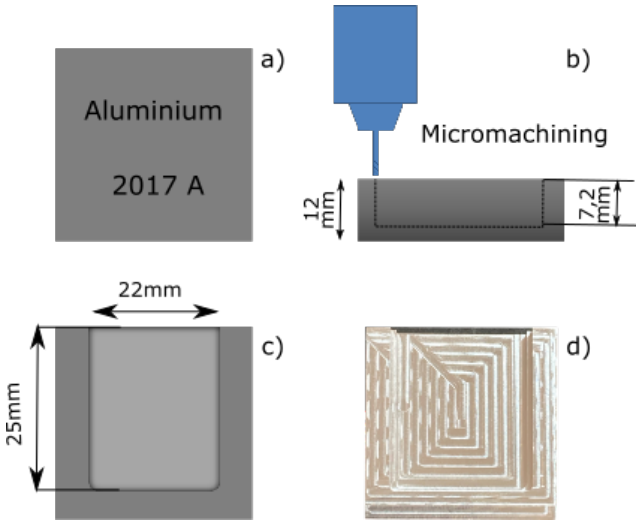

Figure 1: Mold preparation. A parallelepipedic block of Aluminum 2017A (a) is micromachined to prepare a 7.2 mm deep cavity (b) of lateral sizes 22 mm×25 mm (c). (d): picture of the final mold.

of slides serves to increase the bending rigidity of the glass lid, thus avoiding any deviation from planeity of the final PDMS sample that would be simply due to a non-planar lid. Note that the milled cavity reached one of the sides of the aluminum block, thus enabling filling of the cavity with the fluid PDMS mixture from that side (see Fig. 2).

Sylgard 184 silicone elastomer is supplied as a two-parts liquid component kit: a pre-polymer base (part A) and a curing agent (part B). When mixed together, the obtained liquid is curable either at room temperature or at elevated temperatures ($T_{room} < T < 150\,°C$) according to the Sylgard 184 Technical Data Sheet [33]. All PDMS test samples fabricated were mixed at the recommended mass ratio of 10 parts of base to 1 part of curing agent. To ensure standardization and repeatability across all test samples, the mixing process was performed using a commercial mechanical stirrer (IKA Ministar 40). All samples were thoroughly mixed for a duration of 10 min at a speed of 500 rpm. In order to fabricate bubble free test samples, the mixed uncured PDMS was thoroughly degassed in a vacuum dessicator at low pressure for at least 30 min using a vacuum pump, until the mixture shows no more air bubbles. The very same degassed PDMS mixture was then poured into two containers, for two different measurements (see below): (i) the aluminum mold described in the previous paragraph (and closed with its glass lid) and (ii) a petri dish (diameter 54 mm).

In this section, we consider single step curing protocols. We tested three different combinations of temperature and curing time: (i) 48 h at 25°C (as suggested in [33]), (ii) 5 h30 at 50°C (two realizations) and (iii) 1 h30 at 80°C. At the end of the curing phase, the parallelepipedic PDMS sample is demolded by carefully removing the aluminum mold, which leaves the sample stuck on the first glass plate of the stack (see Fig. 2). The exposed PDMS surface parallel to the glass plate, denoted from here and below as the "free surface", is the one on which planeity measurement were performed.

2.2. Measurements

For each curing protocol, the cross-linked PDMS hardness was measured on the wafer-like sample molded in the Petri dish, using a commercial Shore A durometer (Shore Instrument & MFG. Co. INC. New York U.S.A. Durometer Type A ASTM D 2240). All hardness measurements were recorded as soon as complete indentation is established, to mitigate against the subsequent relaxation of the elastomer. Each datapoint is the mean value over five measurements, each made at a different location along the sample's surface. Second, the topography of an about 17 mm×17 mm central region of the free surface of the parallelepipedic sample was measured using an optical interferometric profilometer (Bruker Contour GT K1), with a xy frame aligned with the sides of the parallelepipedic sample.

The topographies were analyzed through the following steps (see Fig. 3), by first using Mountains Maps software. First, a region of interest (ROI) of 14 mm×14 mm was cropped out of the raw topography (Fig. 3(a)), with its center matching the center of the mold cavity (identifiable by a slight topography defect due to the milling initiation). The aberrants points, inherent to any interferometric techniques, (scattered white points in Fig. 3(a)) were removed using the tool "remove outliers". The topography was then flattened by removing its average plane, and a central square sub-region (in white in Fig. 3(a)) was further discarded due to the presence of the above-mentioned milling defect. We then continue our analysis by using Matlab software. The flattened topography was fitted with an elliptic paraboloid whose axis of symmetry is parallel to the z-axis, defined by the equation $z = z_0 + \frac{x'^2}{2R_1} + \frac{y'^2}{2R_2}$. z_0 is a non-physical vertical offset, which was then removed from all subsequent steps, thus defining a vanishing altitude at the apex of the fitted paraboloid. The iso-altitudes of the paraboloid are ellipses (see Fig. 3(b)), the principal axes of which define the in-plane x' and y' axes, that are orthogonal to each other, but rotated by an angle θ with respect to the natural x and y axes of the acquired topographies (see Fig. 3(b)). R_1 and R_2 ($R_1 < R_2$) correspond to the main radii of curvature of the paraboloid, at its apex, along the x' and y' axes, respectively. A directly related, but maybe

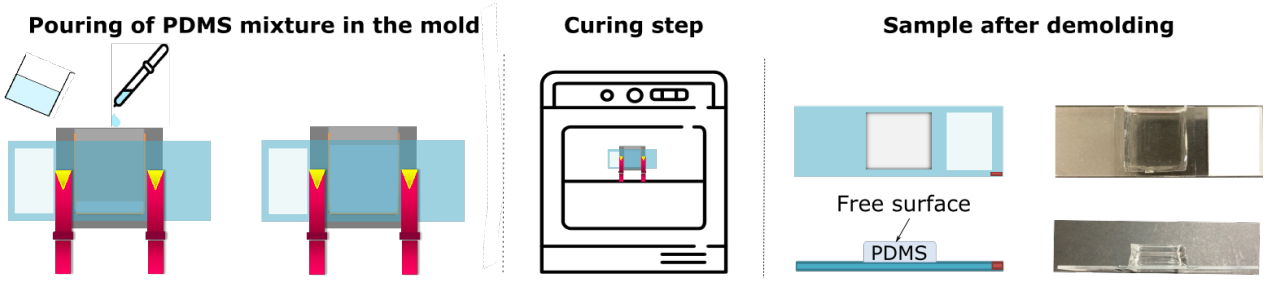

Figure 2: PDMS sample preparation. The aluminum mold (grey part, same as in Fig. 1) is closed by a stack of three glass plates, and the liquid PDMS mixture is poured from top. After curing, the sample is carefully demolded, while remaining attached to one of the glass plates. The free surface on which profilometry measurements are performed is indicated on the bottom left sketch. Rightmost column: pictures of a typical sample.

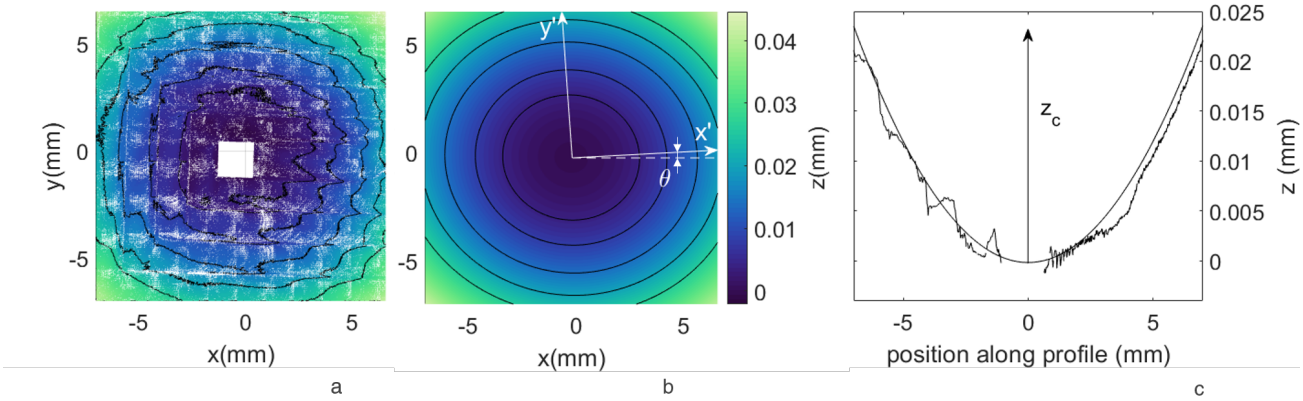

Figure 3: Topography analysis (illustrated on the sample cured with a single-step protocol at 80 °C). (a) Cropped topography, from which the average plane has been removed. Discarded points are in white (aberrant points and central square). Black lines: iso-altitude curves at z=4, 8, 14, 20 and 26 μm. (b) Fitted paraboloid, with the same iso-altitude curves (ellipses) as in (a). Definition of the principal axes, x' and y', and their angle θ with respect to the (x, y) frame. (c) Cut across the fitted paraboloid along the x' axis, superimposed with the corresponding cut across the experimental topography. z_c is illustrated.

more intuitive, estimator of the planeity error was also computed as the altitude z_c reached by the fitted paraboloid at a location such that $x' = 7\,\text{mm}$ (half of ROI lateral size) and $y' = 0\,\text{mm}$. z_c is illustrated on Fig. 3(c), where a typical experimental topography profile along the x' axis is shown, together with the corresponding profile of the fitted paraboloid. One can see that choosing a paraboloid to fit our experimental data gives reasonably good results, which is confirmed by a large goodness of fit as indicated by R^2 values larger than 0.975 for curing temperatures 50 and 80 ° (for 25 °, the shape error being very small, the signal to noise ratio is weak, thus yielding a much poorer fitting quality). Also note that the paraboloid apex is always found reasonably close to the center of the ROI ($x = y \simeq 7\,\text{mm}$ in Fig. 3(b)).

The evolution of the smallest radius of curvature, R_1, and of the altitude error, z_c, are plotted in Fig. 4(a) as a function of the curing temperature. A planeity error is robustly found, which decreases as the curing temperature decreases: z_c is as high as 24 μm ($R_1 \simeq 1\,\text{m}$) at 80 °C, but drops to z_c as small as about 3 μm ($R_1 \simeq 7.8\,\text{m}$) at 25 °C. Note that, at 50 and 80 °C, R_1 and R_2 are almost equal, indicating a residual shape of the free surface being axi-symmetric around the point ($x' = 0, y' = 0$). In constrast, at 25 °C, we find an anisotropic topography, with $R_2 \simeq 5R_1$, i.e. the surface is very flat along the y' axis. For a more intuitive assessment of the planeity errors, Fig.4(b) shows the x' profiles of the fitted paraboloids for all experiments performed.

Importantly, we checked that the planeity error on the PDMS' free surface does not come from an unwanted shape of either the milled aluminum mold, or of the glass lid. To do that, we first measured the topography of the excavated face of mold, and applied the exact same analysis as for the PDMS surface. We found $R_1 \simeq 8.1\,\text{m}$ and $R_2 >> R_1$,

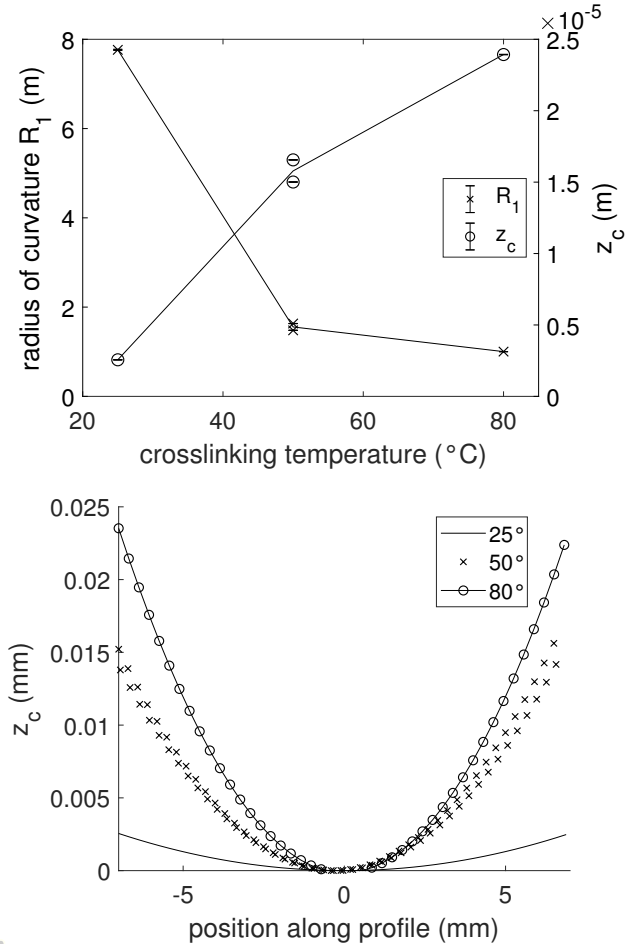

Figure 4: Top: evolution of R_1 (left axis) and z_c (right axis) as a function of the curing temperature. Bottom: profiles along x' (showing the smallest radius of curvature, R_1) of the fitted paraboloid of the PDMS's free surface, for the various tested single-step protocols. For each case, z_c is directly readable as the largest altitude reached on this plot.

two features that closely match the results found on the PDMS' free surface after curing at 25 °C. Such a matching strongly suggests that the residual shape found at 25 °C is not a replication error, but a faithful replication of a non perfectly flat aluminum mold. This conclusion is further substantiated by our second topography measurement, made on the lid in its clamped position (to account for possible bending effect due to clamping). Indeed, in that case, we find that the topography has a Root Mean Square Error (RMSE) of only about 25 nm with respect to a perfect plane, thus excluding any artifact due to the lid.

From those results, one may naïvely believe that a simple solution to practically eliminate planeity errors during molding is to cure the sample at room

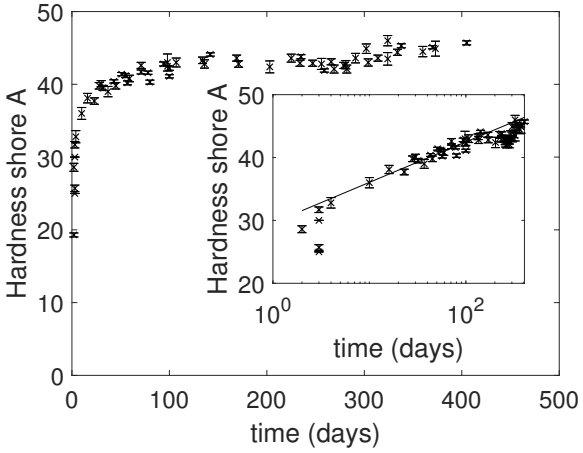

Figure 5: Evolution of the hardness as a function of cross-linking time at 25 °C. The data include different samples made using different batches. Inset: same data in semi-logarithmic scales. Line: guide for the eye indicating a logarithmic trend.

temperature. However, the question remains whether such a single-step protocol ensures completion of the cross-linking reaction. This is why we have performed a study of the evolution of the sample hardness as a function of the curing time at 25 °C. The results are shown on Fig. 5, over a total time longer than a year. As one can see from the alignment of the points in semi-logarithmic scale (inset of Fig. 5), the hardness increases logarithmically with curing time, until reaching a plateau at about 43 shore A. This plateau is not reached before about 100 days, which is a very inconvenient time for sample preparation, much longer than any time used in the protocols from the literature. In particular, a hardness of only about 29 shore A is reached after 48 h at 25 °C. Note that the hardness plateau was found to depend slightly on the cross-linking temperature: about 47 shore A for curing 5h30 at 50 °C (42 is reached right after those 5h30), and about 50 shore A for curing 1h30 at 80 °C (46 is reached right after those 1h30).

In this context, we looked for a cross-linking protocol that would both avoid replication errors and reach full cross-linking within at most a couple of days. We got inspiration from the study of Wong [34], who proposed a two-steps protocol to avoid global curvature of PDMS sample cured in a temperature gradient.

3. Solution protocol

After trial and error, we found that the following two-steps curing protocol offers a good replication quality within less than 17 hours. It consists of (i) a first curing step at 25 °C for 15 h, (ii) demolding, and (iii) a second

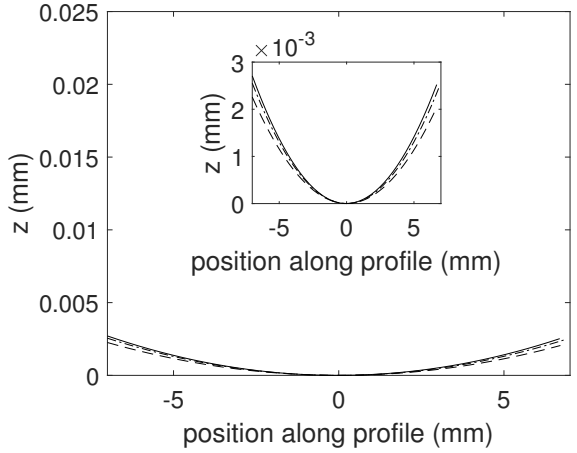

Figure 6: Profiles along x' of the fitted paraboloid of the PDMS's free surface, for various protocols (same z range as in Fig. 4). Inset: zoom on the same data. Solid line: single-step protocol of 48 h at 25°C. Dashed line: recommended two-steps protocol of Sec.3 (15 h at 25°C and 1.5 h at 80°C). Dash-dotted line: alternative two-steps protocol mentioned in Sec. 4 (15 h at 25°C and 4 h at 50°C).

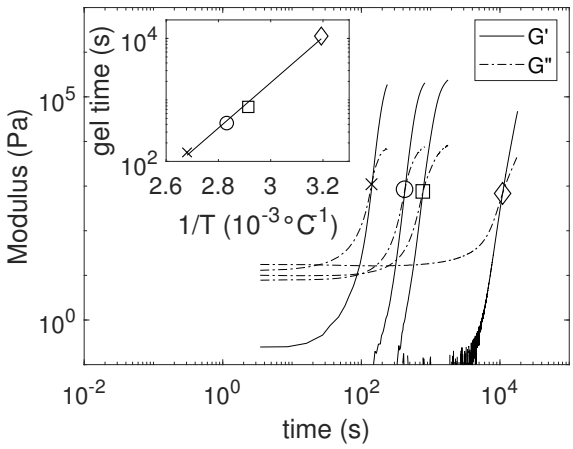

Figure 7: Main: Evolution of the viscoelastic moduli, G' and G'', as a function of the cross-linking time, for various curing temperatures (40, 70, 80 and 100 °C, for the curves from right to left), in log-log scales. Inset: estimated gel time as a function of the inverse of the curing temperature, in semi-log scales. Line: exponential fit.

curing step at 80 °C for 1.5 h.

This enhanced protocol was found to produce very small residual shapes, characterized by $R_1 \simeq 11.7$ m, $R_2 \simeq 32.1$ m, $z_c \simeq 2.4\,\mu$m (see Fig. 6). Those values are very similar to that obtained for the single step protocol at 25°C (see Sec. 2.2 and Fig. 4). Its advantage is that it ensures a final hardness already on the plateau at 43 shore A, indicating a fully completed cross-linking reaction, after a protocol duration of only 17 h.

4. Discussion/justification of protocol

The rationale behind our solution protocol is the following, and is similar to that discussed in [34]. As seen in the previous section, to avoid/minimize replication errors, we need to cure the sample at the temperature at which it will be subsequently used. This is why the first step is a curing step at 25°C. The duration of this first step needs to be long enough for the sample to reach a stable macroscopic shape, while remaining as short as possible, for the sake of sample production logistics. The point at which a cross-linking PDMS sample switches from a liquid-dominated behaviour to a solid-dominated one is the so-called gel point [35]. The gel point is commonly estimated as the point at which, during cross-linking, the storage and loss moduli of the material, G' and G" respectively, become equal [36].

To determine the time at which the gel point is reached, we monitored the kinetics of solidification of the continuous phase using oscillating shear rheology (AR 2000 rheometer by TA Instrument). We used a plane-conical geometry (cone radius, angle and truncation are 20 mm, 4° and 111 μm, respectively), and measured both G' and G" every 10 s with oscillations of amplitude of 0.5%, and a frequency of 1 Hz. Figure 7 shows the evolution of G' and G'' as a function of the cross-linking time, for four different cross-linking temperatures: 40, 70, 80 and 100°C. Note that these results agree quantitatively with those of [37]. As expected, the gel point is reached after a shorter time for larger temperatures. Note that the origin of time in this analysis is taken as the instant at which the target temperature is reached in the rheometer, i.e. after about an incompressible 1h30 dedicated to mixture, degassing, transport to the rheometer and heating ramp to the target temperature.

The inset of Fig. 7 represents the gel time, GT, as a function of cross-linking temperature. As emphasized by the semi-log representation, the gel time *vs* temperature evolution is well captured by an Arrhenius law (also see [38]) of the type $GT \sim e^{\frac{E_a}{RT}}$, where R is the universal gas constant, T is the absolute cross-linking temperature and E_a is the cross-linking activation energy. Extrapolation of the fitted Arrhenius law (see solid line in inset of Fig. 7) to 25°C enables estimating the gel time associated with a cross-linking at 25°C to about 11 h. This value is smaller than the 15 h of the first curing step, strongly

suggesting that, indeed, the PDMS sample is already solidified at the end of this first step. This is confirmed by the fact that demolding is usually fully possible at that stage. In some instances, and depending on the PDMS batch and air moisture, the sample was still found slightly sticky after a first curing step of 15 h at 25 °. In those cases, the first curing step was extended to 24 h, which proved to solve the issue without any observable effect on the final hardness. We expect that this conservative value of 24 h will ensure safe replication in a wide range of atmospheric conditions, and irrespective of the PDMS batch.

The role of the second curing step at a higher temperature of 80 °C is then to complete the cross-linking reaction within a much shorter time than the 100 days that would be necessary at 25 °C (see Fig. 5). This acceleration of the reaction proved to be efficient, without generating any additional replication error. Completion of the cross-linking reaction was indicated by a hardness very close to the plateau value (43 shore A) while, after the first curing step, it was smaller than 29 shore A (the value after 48 h at 25 °C, already mentioned earlier).

Note that an alternative second step has been tested, corresponding to a curing of 4 h at 50 °C. It led to similarly small replication errors (see Fig. 6). However, the duration of 4 h was not sufficient to fully reach completion of the cross-linking reaction, as indicated by a hardness of 39 shore A. We believe that a duration of 8 h for such a second curing step at 50 °C would prove sufficient to reach the final hardness.

It is interesting to note that the moment at which demolding is performed is also important. Indeed, for a second curing step of 2 or 4 h at 50 °C, when demolding only after the second curing step, we found replication errors $z_c \simeq 9.4\,\mu$m, significantly larger than what was found when demolding between the two curing steps ($z_c \simeq 2.9\,\mu$m). We currently lack an explanation for this observation.

5. Origin of replication errors

As we have seen, the observed replication errors appear to be directly related to the curing temperature used to reach the gel time ; in addition, those errors vanish when the curing temperature is equal to the final operating temperature of the PDMS sample. In this context, we hypothesize that the observed shape errors are related to the thermal contraction occurring when cooling the sample from the curing temperature down to room temperature. To test this hypothesis, we performed static finite element calculations of such thermal contraction, using the 'Mechanical' tool within the Ansys software.

A parallelepipedic solid of thickness 7.2 mm and

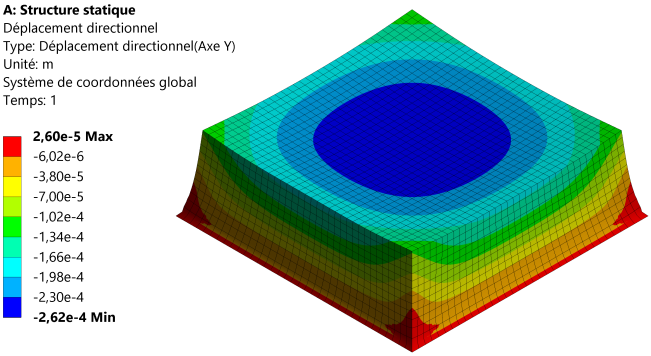

Figure 8: Reference Finite Element simulation: Cooling of a parallelepipedic PDMS block, stuck to a rigid surface at its bottom boundary, from 80 °C down to 20 °C. The color code indicates vertical displacement, in m, from red (zero displacement at the reference bottom boundary) to blue (maximum downward/negative displacement).

a square base of lateral size 21 mm is meshed with rectangular cuboid elements (see Fig. 8). They possess 8 nodes per face and 3 degrees-of-freedom per node, corresponding to translations in the three directions. Their characteristic size is 0.6 mm (a value that we checked to be small enough to ensure convergence of the calculations) so that the model contains a total of 14790 elements and 195480 degrees of freedom. The elements are used with homogeneous, isotropic, linear elastic solid behaviour. The Poisson's ratio, Young's modulus and coefficient of linear thermal expansion are taken equal to typical values for Sylgard 184 PDMS: respectively 0.49 [39, 40], 1.6 MPa (as measured independently from the relationship between contact area and normal load of a PDMS sphere/glass plane, using Hertz' contact model [41] ; method and values similar to [12]) and $3.2\times10^{-4}\,°\mathrm{C}^{-1}$ [40]. The parallelepiped faces are all stress-free, except for the bottom face, the nodes of which are fixed to their initial position, to model the fact that, in the experiments, the sample is stuck to its rigid glass plate.

Our reference calculation simply corresponds to a drop of temperature from 80 °C (the curing temperature) down to 20 °C (a reasonable estimate of the room temperature). As shown in Fig. 8, the initially perfectly parallelepipedic sample ends up having a shape characterized by a concave top surface. Such a feature is in perfect qualitative agreement with our observations of Sec. 2. More quantitatively, we fitted the concave topography of the top surface of the simulated stuck sample, with the same elliptical paraboloid function that we used in Sec. 2 for our experimental samples. Again, the fitting quality is

good ($R^2 = 0.996$) and provides $R_1 = R_2 = 0.68\,\mathrm{m}$, yielding $z_c \simeq 36\,\mu\mathrm{m}$. A similar calculation using an initial temperature of 50 °C instead of 80 °C led to $R_1 = R_2 = 1.38\,\mathrm{m}$ and $z_c \simeq 18\,\mu\mathrm{m}$. Those values are in good quantitative agreement with those found experimentally for single step protocols at the same curing temperatures (see Fig. 4). Such agreement validates our initial hypothesis. We can thus conclude that boundary-frustrated thermal contraction is the phenomenon responsible for the replication errors observed with single-step protocols at a curing temperature higher than the final operating temperature of the sample.

Let us now discuss the implications of thermal contraction being the physical origin of the observed replication errors. The first implication is that, although we started our study focusing on macroscale sample shapes, the effect is actually expected to be active at any length scale. Indeed, imagine the same system as that considered in Fig. 8, but homothetically shrunk by any factor, the final geometrical shape would be exactly the same, in the sense that all sizes in all directions will be scaled down by the same factor. This is illustrated in Fig. 9(top), where the same calculation has been performed on a sample with all sizes divided by a factor of 10. We can see that the exact same shape is recovered, with vertical displacements of the top free surface being ten times smaller than in the reference simulation of Fig. 8. Thus, replication errors due to thermal contraction are generically expected, irrespective of the length scale of the sample.

The second implication is that a change in the aspect ratio of the sample will affect the shape error. As an example, we performed a simulation in which the sample thickness has been divided by 10, while the lateral sizes were kept unchanged. As one can see in Fig. 9(middle), the final shape is now very different from the reference case of Fig. 8. The top free surface is now essentially flat over a large central region, while deviations from planeity are localized around the periphery of the sample. Such a shape indicates that the planeity error on a parallelepipedic sample is an edge effects, affecting the top surface topography only over a lateral size of order the sample's thickness.

The third implication is that the final shape observed in Fig. 8 is fundamentally related to the fact that the PDMS is stuck to the rigid glass plate: at the PDMS/glass interface, no displacement is allowed, which impedes the homothetic size-change of the sample that would occur if the sample was free of any boundary constraint. This conclusion is substantiated by the results of a last calculation (Fig. 9(bottom)), which is the same as the reference one, except that the bottom face is also stress-free. As can be seen, the sample keeps its parallelepipedic shape, and only

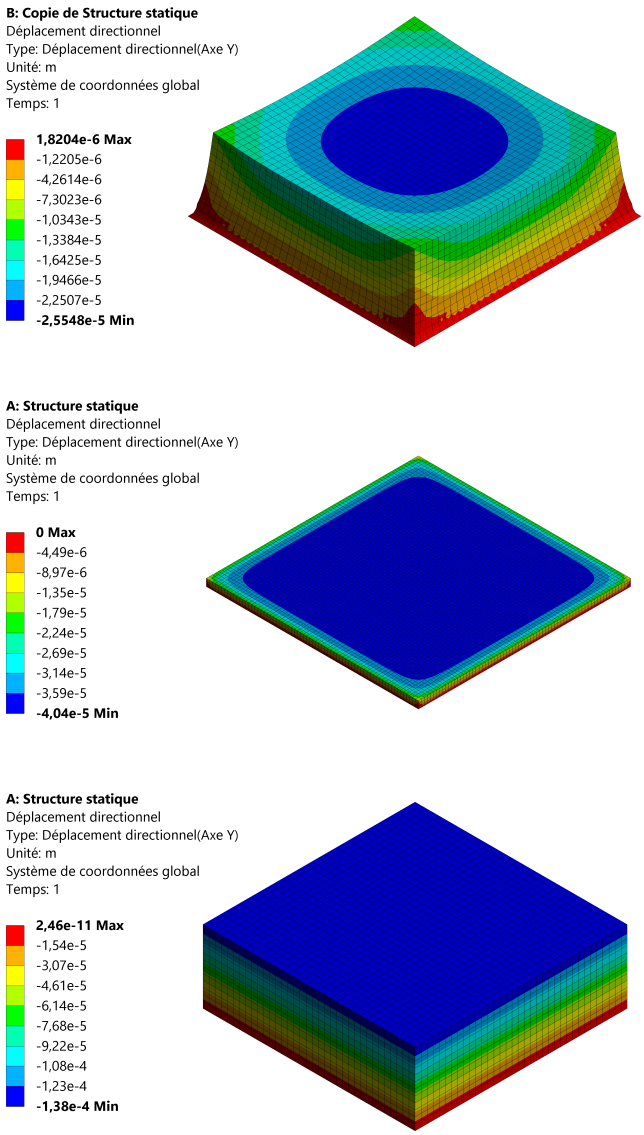

Figure 9: Additional Finite Element simulations. Top: same as reference simulation of Fig. 8, but for a sample with all dimensions divided by a factor of 10. Middle: same as reference simulation, but for a sample with a thickness divided by a factor of 10. Bottom: same as reference simulation, but when all faces are stress-free.

shrinks isotropically.

Note that sample shrinkage associated with PDMS curing at higher-than-room-temperature had previously been investigated in relation with replication. For instance, for fully demolded samples, it was shown to be responsible for too small sample dimensions, by up to a few percents, an effect possibly compensated by using a mold adequately larger than the final desired size [20, 42]. The same effect was also found responsible for global curvature in fully demolded samples cured in a temperature gradient on a hot plate [34]. We emphasize that, here, we showed that the effect is also relevant for samples submitted to a homogeneous curing temperature (in an oven), and which are not fully demolded but remain stuck on a rigid substrate. Finally, in another context, the same thermal effect, which is a problem for replication, has instead been taken advantage of in Ref. [40] to measure the Poisson ratio and coefficient of thermal expansion of PDMS Sylgard 184.

Finally, also note that we observed an additional evolution of the sample shape over very long timescales (typically months), characterized by an increase of z_c (by typical amounts of a few μm) and a reduction of the anisotropy of the planeity error, when any. Such aging of the samples occurs at constant, room temperature, and is thus of a different physical origin from that relevant during the initial curing protocol. Explaining the origin of such aging is beyond the scope of the present work, but may constitute an interesting topic for future studies.

6. Conclusion

In this work, we questioned the replication quality of samples with a nominally flat surfaces using PDMS Sylgard 184. We first showed that most of the single-step curing protocols used in the literature yield planeity errors of typical order tens of micrometers out-of-plane over 1 cm along the plane (Sec. 2). Such errors are expected to be generally problematic, in particular for all applications in which the surface needs to be brought into contact with another flat solid, like in tribology [16] or in microfluidics [43].

We showed that this effect arises when the thermal contraction of the PDMS sample, when cooling from its curing temperature down to its final operating temperature, is frustrated by some mechanical constraint (Sec. 5). In our case, frustration was due to the fact that the sample was molded directly on its final rigid substrate (a glass plate). As a counter-measure, we have identified a two-steps curing protocol (described in Sec. 3) that enables faithful mold replication. Its main features are first to reach the gel point of the PDMS through an initial curing step at the final operating temperature, and then to complete cross-linking within a reasonable time through a higher-temperature second curing step.

The two-steps protocol of Sec. 3 will be useful in any situation in which a good control of the sample's shape is required. Identifying thermal contraction as the physical origin of the identified replication error implies that those errors are expected at any length scale, and that they strongly depend on the sample's aspect ratio and boundary conditions. Although our results have been obtained on parallelepipedic samples, we expect that the insights brought will be useful to develop mitigation strategies against replication errors that will be suitable in any other sample geometry.

Acknowledgements

This work has been funded by the French ANR, through grant ANR-18-CE08-0011-01 (project PROMETAF).

Bibliography

[1] E. Menard and J. A. Rogers. Stamping Techniques for Micro- and Nanofabrication. In B. Bhushan, editor, *Springer Handbook of Nanotechnology*, pages 313–332. Springer, Berlin, Heidelberg, 2010.

[2] C. Con and B. Cui. Effect of mold treatment by solvent on PDMS molding into nanoholes. *Nanoscale Research Letters*, 8(1):394, 2013.

[3] J. S. Persson, A. Tiwari, E. Valbahs, T. V. Tolpekina, and B. N. J. Persson. On the Use of Silicon Rubber Replica for Surface Topography Studies. *Tribology Letters*, 66(4):140, 2018.

[4] D. Pérez-Calixto, D. Zamarrón-Hernández, A. Cruz-Ramírez, M. Hautefeuille, J. Hérnandez-Cordero, V. Velázquez, and M. Grether. Fabrication of large all-PDMS micropatterned waveguides for lab on chip integration using a rapid prototyping technique. *Optical Materials Express*, 7(4):1343–1350, 2017.

[5] H. Chai, F. Chen, Z. Song, L. Xiong, G. Xiao, Z. Lu, and L. Yu. A versatile wax assisted double replica molding and its application in flexible electronic skin. *Sensors and Actuators B: Chemical*, 343:130132, 2021.

[6] J. C. McDonald and G. M. Whitesides. Poly(dimethylsiloxane) as a Material for Fabricating Microfluidic Devices. *Accounts of Chemical Research*, 35(7):491–499, 2002.

[7] K. Raj M and S. Chakraborty. PDMS microfluidics: A mini review. *Journal of Applied Polymer Science*, 137(27):48958, 2020.

[8] J. Scheibert, S. Leurent, A. Prevost, and G. Debrégeas. The Role of Fingerprints in the Coding of Tactile Information Probed with a Biomimetic Sensor. *Science*, 323(5920):1503–1506, 2009.

[9] G. M. Whitesides. Soft Robotics. *Angewandte Chemie International Edition*, 57(16):4258–4273, 2018.

[10] H. Tao and J. Gibert. Multifunctional Mechanical Metamaterials with Embedded Triboelectric Nanogenerators. *Advanced Functional Materials*, 30(23):2001720, 2020.

[11] A. Prevost, J. Scheibert, and G. Debrégeas. Probing the micromechanics of a multi-contact interface at the onset of frictional sliding. *The European Physical Journal E*, 36(2), 2013.

[12] R. Sahli, G. Pallares, C. Ducottet, I. E. Ben Ali, S. Al Akhrass, M. Guibert, and J. Scheibert. Evolution of real contact area under shear and the value of static friction of soft materials. *Proceedings of the National Academy of Sciences of the USA*, 115:471–176, 2018.

[13] V. Acito, M. Ciavarella, A. M. Prevost, and A. Chateauminois. Adhesive Contact of Model Randomly Rough Rubber Surfaces. *Tribology Letters*, 67(2):54, 2019.

[14] V. Tinnemann, L. Hernández, S. C. L. Fischer, E. Arzt, R. Bennewitz, and R. Hensel. In Situ Observation Reveals Local Detachment Mechanisms and Suction Effects in Micropatterned Adhesives. *Advanced Functional Materials*, 29(14):1807713, 2019.

[15] H. Schmid and B. Michel. Siloxane Polymers for High-Resolution, High-Accuracy Soft Lithography. *Macromolecules*, 33(8):3042–3049, 2000.

[16] V. Romero, E. Wandersman, G. Debrégeas, and A. Prevost. Probing Locally the Onset of Slippage at a Model Multicontact Interface. *Physical Review Letters*, 112(9):094301, 2014.

[17] A. O'Neill, J. Soo Hoo, and G. Walker. Rapid curing of PDMS for microfluidic applications. *Chips and Tips*. Blog page published on 23/10/2006, readable on https://blogs.rsc.org/chipsandtips/2006/10/23/rapid-curing-of-pdms-for-microfluidic-applications/ (consulted on 19/05/2021).

[18] T. G. Oyama, K. Oyama, and M. Taguchi. A simple method for production of hydrophilic, rigid, and sterilized multi-layer 3D integrated polydimethylsiloxane microfluidic chips. *Lab Chip*, 20(13):2354–2363, 2020.

[19] Y. S. Shin, K. Cho, S. H. Lim, S. Chung, S.-J. Park, C. Chung, D.-C. Han, and J. K. Chang. PDMS-based micro PCR chip with Parylene coating. *Journal of Micromechanics and Microengineering*, 13(5):768–774, 2003.

[20] S. W. Lee and S. S. Lee. Shrinkage ratio of PDMS and its alignment method for the wafer level process. *Microsystem Technologies*, 14(2):205–208, 2008.

[21] B.-H. Jo, L.M. Van Lerberghe, K.M. Motsegood, and D.J. Beebe. Three-dimensional micro-channel fabrication in polydimethylsiloxane (PDMS) elastomer. *Journal of Microelectromechanical Systems*, 9(1):76–81, 2000.

[22] K. G. Klemic, J. F. Klemic, and F. J. Sigworth. An air-molding technique for fabricating PDMS planar patch-clamp electrodes. *Pflügers Archiv*, 449(6):564–572, 2005.

[23] Y.-S. Cherng and G.-D. J. Su. Fabrication of polydimethylsiloxane microlens array on spherical surface using multi-replication process. *Journal of Micromechanics and Microengineering*, 24(1):015016, 2013.

[24] J. Nase, A. Lindner, and C. Creton. Pattern Formation during Deformation of a Confined Viscoelastic Layer: From a Viscous Liquid to a Soft Elastic Solid. *Physical Review Letters*, 101(7):074503, 2008.

[25] V. Barreau, R. Hensel, N. K. Guimard, A. Ghatak, R. M. McMeeking, and E. Arzt. Fibrillar Elastomeric Micropatterns Create Tunable Adhesion Even to Rough Surfaces. *Advanced Functional Materials*, 26(26):4687–4694, 2016.

[26] C. Y. Wu, T. H. Chiang, and C. C. Hsu. Fabrication of microlens array diffuser films with controllable haze distribution by combination of breath figures and replica molding methods. *Optics Express*, 16(24):19978–19986, 2008.

[27] G. Vozzi, C. J. Flaim, F. Bianchi, A. Ahluwalia, and S. Bhatia. Microfabricated PLGA scaffolds: a comparative study for application to tissue engineering. *Materials Science and Engineering: C*, 20(1):43–47, 2002.

[28] H.-B. Liu and H.-Q. Gong. Templateless prototyping of polydimethylsiloxane microfluidic structures using a pulsed CO2laser. *Journal of Micromechanics and Microengineering*, 19(3):037002, 2009.

[29] Y. Gombert, R. Simič, F. Roncoroni, M. Dübner, T. Geue, and N. D. Spencer. Structuring Hydrogel Surfaces for Tribology. *Advanced Materials Interfaces*, 6(22):1901320, 2019.

[30] X. Zhu, H. Chen, L. Zhu, H. Wang, and W. Zhang. Fabrication of curved microlens array using a drop-on-demand droplet generator and polydimethylsiloxane replica mold. *Optical Engineering*, 53(11):1–9, 2014.

[31] A. Kumar, H. A. Biebuyck, and G. M. Whitesides. Patterning Self-Assembled Monolayers: Applications in Materials Science. *Langmuir*, 10(5):1498–1511, 1994.

[32] A. Rosenthal, A. Macdonald, and J. Voldman. Cell patterning chip for controlling the stem cell microenvironment. *Biomaterials*, 28(21):3208–3216, 2007.

[33] SYLGARD™ 184 Silicone Elastomer Kit Technical Data Sheet. downloadable from https://www.dow.com/en-us/document-viewer.html?ramdomVar=6028251085099047358&docPath=/content/dam/dcc/documents/en-us/productdatasheet/11/11-31/11-3184-sylgard-184-elastomer.pdf (consulted on 01/07/2021).

[34] E. J. Wong. *Modeling and control of rapid cure in polydimethylsiloxane (PDMS) for microfluidic device applications*. PhD thesis, Massachusetts Institute of Technology, 2010.

[35] H. H. Winter. Gel Point. In *Encyclopedia of Polymer Science and Technology*, pages 1–15. American Cancer Society, 2016.

[36] C.-Y. M. Tung and P. J. Dynes. Relationship between viscoelastic properties and gelation in thermosetting systems. *Journal of Applied Polymer Science*, 27(2):569–574, 1982.

[37] A. Giustiniani. *Linking Adhesive Properties and Pore Organisation of Silicone Emulsions Obtained by Reactive Blending*. PhD thesis, Université Paris Saclay, 2017.

[38] L. Payet, A. Ponton, F. Agnely, P. Colinart, and J. L. Grossiord. Caractérisation rhéologique de la gélification d'alginate et de chitosane : effet de la température. *Rhéologie*, 2:46–51, 2002.

[39] J. Lengiewicz, M. de Souza, M. A. Lahmar, C. Courbon, D. Dalmas, S. Stupkiewicz, and J. Scheibert. Finite deformations govern the anisotropic shear-induced area reduction of soft elastic contacts. *Journal of the Mechanics and Physics of Solids*, 143:104056, 2020.

[40] A. Müller, M. C. Wapler, and U. Wallrabe. A quick and accurate method to determine the Poisson's ratio and the coefficient of thermal expansion of PDMS. *Soft Matter*, 15(4):779–784, 2019.

[41] V. L. Popov. *Contact Mechanics and Friction*. Springer Berlin Heidelberg, 2017.

[42] M. H. Madsen, N. A. Feidenhans'l, P.-E. Hansen, J. Garnæs, and K. Dirscherl. Accounting for PDMS shrinkage when replicating structures. *Journal of Micromechanics and Microengineering*, 24(12):127002, 2014.

[43] U. Abidin, N. A. S. M. Daud, and V. Le Brun. Replication and leakage test of polydimethylsiloxane (PDMS) microfluidics channel. *AIP Conference Proceedings*, 2062(1):020064, 2019.